

# Relocation of aftershocks, focal mechanisms and stress inversion: Implications toward the seismo-tectonics of the causative fault zone of Mw7.6 2001 Bhuj earthquake (India)

P. Mandal <sup>a,\*</sup>, S. Horton <sup>b</sup>

<sup>a</sup> National Geophysical Research Institute, Uppal Road, Hyderabad-500007, India

<sup>b</sup> Center for Earthquake Research and Information, Memphis, Tennessee-38152, USA

Received 9 May 2006; received in revised form 25 September 2006; accepted 26 September 2006

Available online 15 November 2006

## Abstract

The HYPODD relocation of 1172 aftershocks, recorded on 8–17 three-component digital seismographs, delineate a distinct south dipping E–W trending aftershock zone extending up to 35 km depth, which involves a crustal volume of 40 km × 60 km × 35 km. The relocated focal depths delineate the presence of three fault segments and variation in the brittle–ductile transition depths amongst the individual faults as the earthquake foci in the both western and eastern ends are confined up to 28 km depth whilst in the central aftershock zone they are limited up to 35 km depth. The FPFIT focal mechanism solutions of 444 aftershocks (using 8–12 first motions) suggest that the focal mechanisms ranged between pure reverse and pure strike slip except some pure dip slip solutions. Stress inversion performed using the *P* and *T* axes of the selected focal mechanisms reveals an N181°E oriented maximum principal stress with a very shallow dip (=14°). The stress inversions of different depth bins of the *P* and *T* axes of selected aftershocks suggest a heterogeneous stress regime at 0–30 km depth range with a dominant consistent N–S orientation of the *P*-axes over the aftershock zone, which could be attributed to the existence of varied nature and orientation of fractures and faults as revealed by the relocated aftershocks.

© 2006 Elsevier B.V. All rights reserved.

**Keywords:** Aftershock activity; Intraplate earthquake; Double-difference location; Focal Mechanism; Stress inversion

## 1. Introduction

Kachchh area lies in the seismic zone V of India, which has experienced two earthquakes of  $M_w \geq 7.7$  within a span of 182 years (Bureau of Indian Standards, 2002; Mandal et al., 2004a,b). In addition, we know that the region has experienced moderate size earthquakes

since 1668 (Rajendran and Rajendran, 2001). The latest 2001 Bhuj earthquake of  $M_w 7.7$  (intensity X+ on MM Scale) occurred along an E–W trending south dipping reverse fault at 23 km depth (Fig. 1). Available fault plane solutions from first motion indicate that both strike–slip and reverse faulting characterize the Kachchh seismic zone (Chung and Gao, 1995). Further, available GPS campaign data suggests very slow strain accumulation (Sridevi et al., 2001). Thus, the most important question related to tectonics of Kachchh to be answered is how the large strains accumulate in this low

\* Corresponding author.

E-mail addresses: [prantikmandal@yahoo.com](mailto:prantikmandal@yahoo.com) (P. Mandal), [horton@memphis.edu](mailto:horton@memphis.edu) (S. Horton).

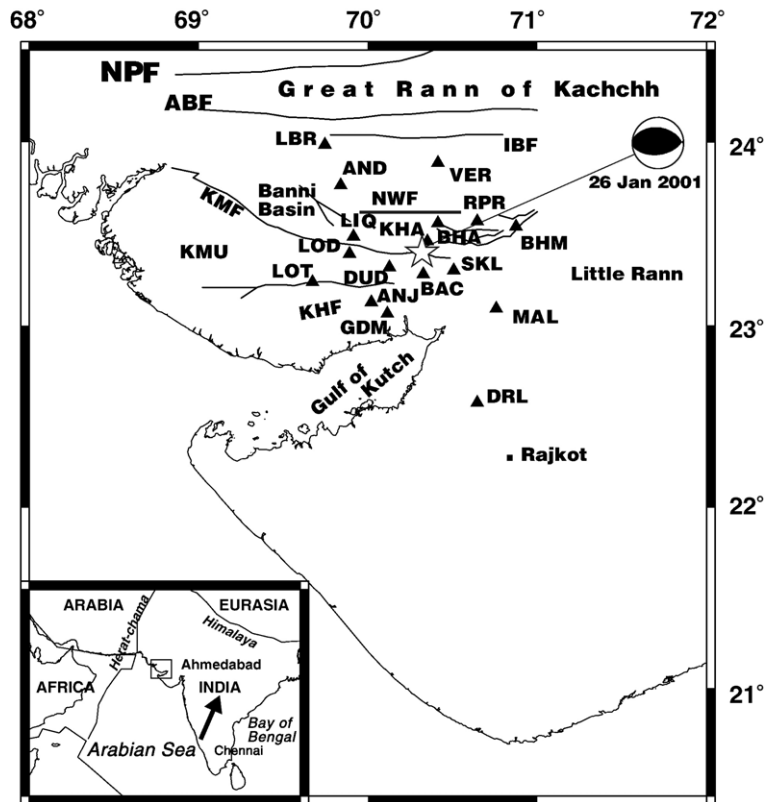


Fig. 1. A plot showing 17 seismograph stations (seismograph stations marked by solid triangles). KU, Kachchh mainland uplift. Major faults (lines): ABF, Allah Bund Fault; IBF, Island belt fault; KMF, Kachchh mainland fault; KHF, Katrol Hill fault; NPF, Nagar Parkar fault; Kathiwar F., Kathiwar Fault; NWF, North Wagad fault. The inset is showing the key map for the area with reference to Indian plate boundaries (dark lines) (After Biswas (1987)). The prevailing compression from in-situ stress measurement and focal mechanism data has been shown by compression arrow symbol (After Gowd et al. (1992)).

strain rate intraplate region (Himalayan plate boundary in the north is more than 1000 km away and Herat–Chaman plate boundary in the west is 500 km away). Hence, the mechanism of stress concentration at the aftershock zone of 2001 Bhuj earthquake, is an important outstanding geodynamic problem, which perhaps can be clarified by focused investigation of the seismotectonics of the causative fault zone using reliable and accurate aftershock data.

Estimation of accurate hypocentral parameters using large aftershock data is becoming an essential tool for understanding the seismotectonics of any seismically active fault zone (Poupinet et al., 1984; Got et al., 1994; Dodge, 1996; Richards-Dinger and Shearer, 2000). Several techniques using the 1-D or 3-D inversion of travel times of P and S waves from local earthquake data have been discussed in the literature for estimating accurate and reliable hypocentral parameters (Thurber, 1983; Michelini, 1991; Michael and Eberhart-Phillips, 1991; Foxall et al., 1993; Zhao et al., 1996; Mandal et al., 2004a,b). These earthquake location techniques

would be generally based on the first order Taylor series approximation of travel time difference between observed and predicted estimates. This linearization approximation would allow earthquakes to be located individually using these algorithms, or jointly with other unknowns related to the location of individual earthquakes, such as station corrections in the joint hypocentral determination (JHD) method, or the velocity model in seismic tomography/simultaneous inversion (Thurber, 1983; Pujol, 1988). In the HYPODD algorithm, the residuals between observed and calculated travel-time difference (double-difference) between two events at a common station are estimated for two very closely spaced events by assuming the similar ray paths between the source region and the common station (Waldhauser and Ellsworth, 2000). This further cancels the common mode errors related to the receiver side structure resulting in no station corrections for the raypath outside the focal volume. The double-difference algorithm (Waldhauser and Ellsworth, 2000) has been extensively used with data from permanent networks

Table 1

1-D Velocity model for the Kachchh, Gujarat obtained from the travel time inversion using VELEST (Mandal, in press)

Depth to the bottom of the layer (km)	Vp (km/s)	Vs (km/s)	Vp/Vs	Geology
2.0	2.92	0.90	3.24	Tertiary sediments
5.0	5.99	3.49	1.72	Jurassic sediments
10.0	5.90	3.37	1.75	Upper crust
16.0	6.18	3.60	1.72	Upper crust
22.0	6.07	3.60	1.69	Upper crust
29.0	6.59	3.73	1.77	Lower crust
34.0	7.20	3.99	1.80	Lower crust
42.0	6.78	3.44	1.97	Lower crust
∞	8.20	4.70	1.74	Half space

and aftershock arrays around the world, where it has demonstrated an ability to improve the image of seismicity in every case studied.

Another parameter for better understanding of the ongoing geodynamical process in a fault zone is a good reliable estimate of the stress tensor (Bott, 1959; McKenzie, 1969). The nature of stress tensor (compressive/extensional) is generally well known for the inter-plate/plate boundary regions (Bott, 1959). However, the stress regime is quite less obvious from the observed geological or geodynamical processes acting in the intra-plate or stable continental areas, which have undergone several deformation episodes in the past. Common methods to measure magnitude and orientation of stress tensor like overcoring and bore hole breakouts can be performed at near surface depths only (McGarr and Gay, 1978). These methods cannot provide any information regarding variation in stress tensor

behavior with depth. Thus, the use of focal mechanism to estimate the nature of stress tensor deep in the crust is becoming more popular (Gephart and Forsyth, 1984). Stress inversion can be performed over a large number of earthquakes for the reliable estimation of stress tensor (Gephart, 1990a,b). The technique provides an estimate for the orientation of the stress tensor, but does not provide any information regarding the magnitudes of the stress tensor. In fact, the stress inversion yields only an aspect ratio that is a measure of the relative importance of the principal deviatoric stresses. The accuracy of these stress inversions is limited, however, by the uncertain reliability of many of the focal mechanism estimates and the fault plane ambiguity inherent in the double-couple source.

In this paper, we present the salient results from our HYPODD relocation, focal mechanism and stress inversion. We used 1238 aftershocks of the 2001 Mw 7.6 Bhuj earthquake recorded by a combined network of the National Geophysical Research Institute (NGRI), Hyderabad, India and CERl, Memphis, USA during 12–28 February 2001. Finally, these results are correlated with the local geology and tectonics with a view to characterize the seismotectonics of the causative fault zone of the 2001 Bhuj earthquake.

## 2. Geology, tectonics and seismicity of the Kachchh region

The Kachchh rift is the largest Indian intracontinental rift zone and is situated at the western border of the India far from any plate boundary (Fig. 1). Geologically,

Table 2

Station coordinates, travel-time corrections, and site conditions

Station	Latitude (°N)	Longitude (°E)	P Correction (s)	S Correction (s)	Geology	Structures
AND	23.7673	69.8388	−0.04	−0.51	Sandstone	Stick hut
ANJ	23.1278	70.0205	+0.06	+0.09	Deeply weathered sandstone	Very small shed
BAC	23.2808	70.3266	+0.01	−0.03	Basalt flow	Free field
BHA	23.5600	70.4141	+0.03	−0.08	Deeply weathered sandstone	Small underground storage room
DUD	23.3195	70.1270	−0.07	−0.12	Weathered sandstone	Ground floor of a damaged 1-story masonry
DRL	22.5770	70.6460			Weathered sandstone	Small 1-story stone hut
GDM	23.0660	70.1150	+0.27	+0.14	Hard sandstone	Small 1-story RCC room of a nursery
KHA	23.4605	73.3516	+0.00	+0.13	Deeply weathered sandstone	Ground floor of damaged 1-story masonry
LBR	23.9875	69.7463	−0.13	−0.07	Slightly indurated sediments	Free field
LIQ	23.4878	69.9153	+0.01	+0.63	Deep consolidated sediment	Free field
LOD	23.3930	69.8920	+0.17	+0.12	Weathered sandstone	Basement of a 2-story stone house
LOT	23.2383	69.6726	+0.10	+0.05	Thin soil over sandstone	Basement of a 2-story stone house
MAL	23.0930	70.7580	+0.37	+0.06	Sandstone	Small 1-story storage room
RPR	23.5708	70.6460	+0.03	−0.06	Hard sediments	Basement of a 2-story stone house
SKL	23.3030	70.5070	+0.23	+0.46	Weathered sandstone	1-story RCC room of a school
VER	23.8888	70.4138	−0.01	−0.05	Sandstone	Thatch hut
BHM	23.5420	70.8750	+0.05	−0.07	Weathered sandstone	Small 1-story stone house

Quaternary/Tertiary sediments, Deccan volcanic rocks and Jurassic sandstones resting on Precambrian basement mainly characterize the Kachchh region (Gupta et al., 2001). The evidence of the Precambrian basement has been seen in the Banni deep well (north of the epicentral zone), where the Precambrian granite porphyry/rhyolite is found at a depth of 1718.5 m (Singh et al., 1997). The Mesozoic rift related extensional structures of the Kachchh basin got reactivated as strike–slip or reverse faults as a result of regional compressive stresses due to collision of Indian and Eurasian plates since Neogene times (Patriat and Achache, 1984; Jaeger et al., 1989). The focal mechanisms of some earthquakes indicate reverse faulting (Chung and Gao, 1995). It is important to note that the region containing

the Kachchh rift is thought to be within the mid-continent stress province where the mean orientation of the maximum compression is N30° E (Gowd et al., 1992).

Major structural features of the Kachchh region include several E–W trending faults/folds as shown in Fig. 1. The rift zone is bounded by a north dipping Nagar Parkar fault in the north and a south dipping Kathiawar fault in the south. Other major faults in the region are the E–W trending Allah Bund fault, Island belt fault, Kachchh mainland fault and Katrol Hill fault. In addition, several NE and NW trending small faults/lineaments are observed (Biswas, 1987). Seismics, gravity and magneto-telluric surveys indicate undulated basement with 2–5 km deep sediments and

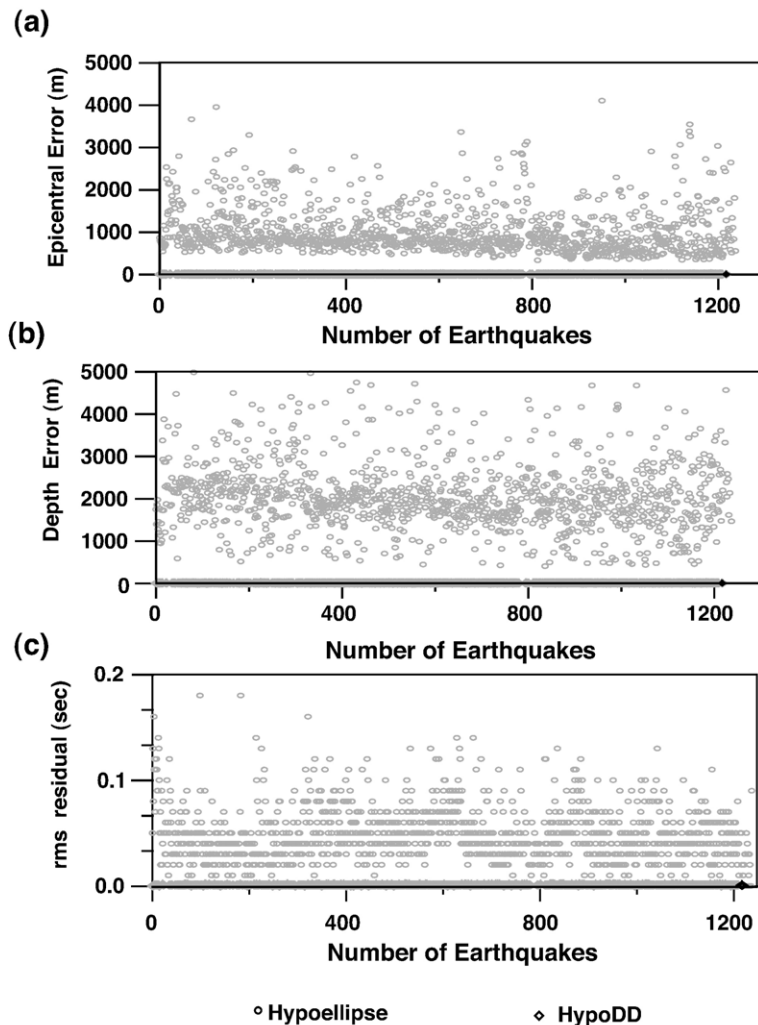


Fig. 2. HYPOELLIPSE location and HYPODD relocation errors of earthquakes (a) epicenter, (b) focal depth, and (c) root mean square value of P-residual.

Moho depth at 35–43 km in southern Kachchh region (Gupta et al., 2001; Reddy et al., 2001). Recently, the analysis and inversion of teleseismic RF suggests a Moho depth variation from 42 to 49 km in the epicentral zone of 2001 Bhuj earthquake (Mandal, *in press*).

The Kachchh region is characterized by large and moderate but infrequent earthquakes. Based on Johnston's (1994) classification scheme, great intraplate earthquakes with  $M_w \geq 7.7$  have occurred in only two intraplate regions in the world: New Madrid, USA and Kachchh, India (Bendick et al., 2001; Bodin et al., 2001; Schweig et al., 2003). Large earthquakes are known to have been occurring in the Kachchh region since historical times (Rajendran and Rajendran, 2001). It has been inferred, based on the radiocarbon dating, that an earthquake occurred between A.D. 885–1035 along the Allah Bund fault (Rajendran and Rajendran, 2001). In 1668, a moderate earthquake occurred west of Kachchh, with an epicenter at  $24^\circ$  N  $68^\circ$  E (Rastogi et al., 2001). The largest earthquake in the region occurred on June 6, 1819. This  $M_w$  7.8 earthquake resulted in a 100 km long ridge and created what is known as the Allah Bund (Johnston, 1994; Rajendran and Rajendran, 2001). Between 1821–1996, 16 moderate earthquakes of magnitude varying from 4.2 to 6.1 have occurred in the region (Rajendran and Rajendran, 2001). The last damaging earthquake of  $M_w$  6.0 (Intensity IX) prior to the most recent  $M_w$  7.7 2001 Bhuj event occurred along the Katrol Hill fault near Anjar, Gujarat in 1956 (Chung and Gao, 1995). This earthquake was apparently a shallow reverse rupture but did not rupture the surface (Chung and Gao, 1995). Most recently there was an earthquake in 1992 (Dodge, 1996), which was  $19 \pm 4$  km deep. On December 24, 2001, an  $M_5$  earthquake struck north of Bhuj, the teleseismically determined epicenter is close to the western end of the Island Belt fault. Whereas, the devastating 2001  $M_w$  7.7 Bhuj earthquake occurred on the ENE–WSW trending and south dipping blind reverse fault (North Wagad Fault) at a depth of 23 km (USGS, Fig. 1). This earthquake had a high static stress drop of 12.6 to 24.6 MPa, over a small circular rupture area with a radius of 20 to 25 km, for a moment of  $4.5 \times 10^{20}$  N-m (Negishi et al., 2001).

### 3. Combined local seismic network

Several institutes from India and other countries deployed their seismic networks in the epicentral area immediately after the occurrence of the  $M_w$  7.6 Bhuj earthquake on 26 January 2001 (Negishi et al., 2001; Mandal et al., 2004a; Bodin and Horton, 2004). In this paper, we combine aftershock data from two of these

seismic networks (National Geophysical Research Institute (NGRI), Hyderabad, India and Center for Earthquake Research and Information (CERI), Memphis, USA) that operated concurrently from 13 to 27 February 2001. Although both data sets have been independently studied, the combined dataset provides P- and S-phase data from 8–16 stations. The increased data

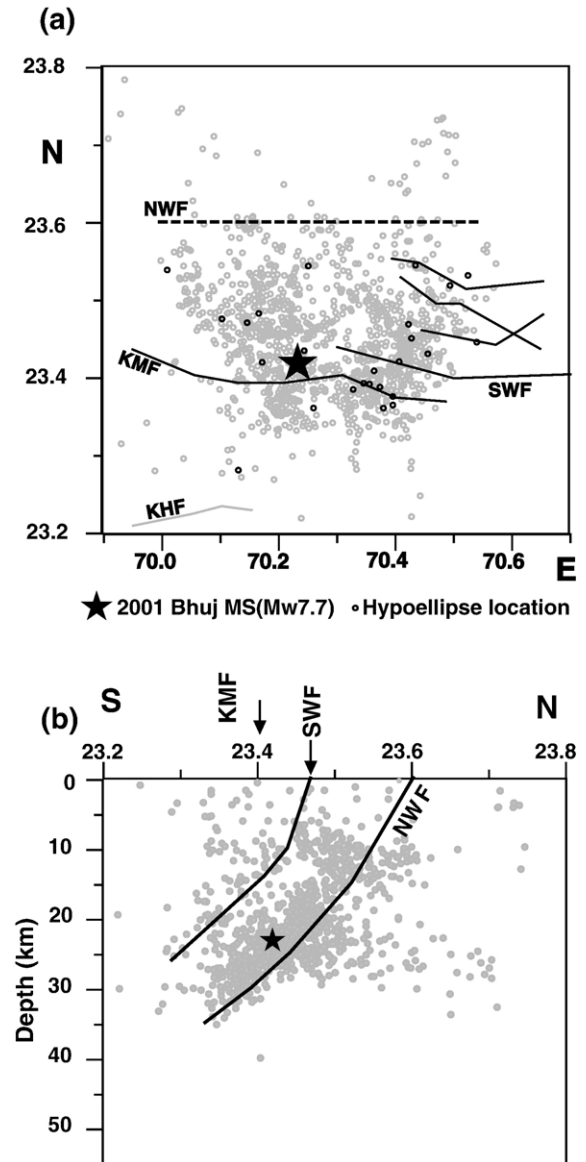


Fig. 3. (a) Epicenters of selected 1238 aftershocks by using HYPOELLIPSE, which have occurred during 12–28 February 2001. A solid star shows the epicenter for the 2001 Bhuj mainshock. The inferred causative fault is shown by dotted line and marked as NWF. (b) Hypocentral depth plots of selected earthquakes in N–S direction (Geologically valid inferred fault trace is shown by dotted line and marked as NWF. Arrows mark surface traces of KMF and SWF (after Biswas (1987)).

coverage can potentially improve location estimates and provide better-constrained focal mechanism solutions.

The local NGRI digital Seismograph network consisted of 8 stations. Each station was comprised of a 24-bit recorder (REFTEK) with a GPS timing system. Six of these were equipped with short period seismometers (Mark Products triaxial L4-3D, Frequency range 1–40 Hz) and two with broadband sensors (Guralp CMG-3ESP, Frequency range 0.01–40 Hz). Recording was done in continuous mode at a sampling rate of 100 sps. CERI deployed eight Kinometrics K2 digital recorders equipped with an internal force-balance accelerometer set to full scale of 2 g and a built-in GPS timing system. Each K2 was also equipped with an external velocity sensor (Mark Products triaxial L-28) to ensure detection of weak ground motion. Data was recorded at 200 sps in a triggered mode.

The station locations of this combined network are listed in Table 1 and shown in Fig. 1. The distance between station and epicenters varies from 14 km to 90 km. This network provides an azimuthal gap of less

than 180°. Most of these stations were located on hard sediments or rocks (Jurassic sediments or basalt). However, few of these stations were sited on a thin layer of soil overlying rock. The network is covered very well in all directions except the northern and central areas due to non-availability of roads in Banni region. The largest aftershocks recorded during the above mentioned period is  $m_b$  5.2 (PDE) and several were  $m_b > 4.0$ .

#### 4. Initial aftershock locations

Initial event locations were obtained using the program HYPOELLIPSE (Lahr, 1995). We used a 1-D velocity model (Table 1) obtained from inversion of travel times of P and S waves using VELEST (Kissling, 1995; Mandal, in press). Travel-time deviations of individual stations from values predicted by this average model were accounted for using station correction terms in the locations. Station corrections based on average travel-time residuals at each station are shown in Table 2. The average location rms was 0.05 s (Fig. 2).

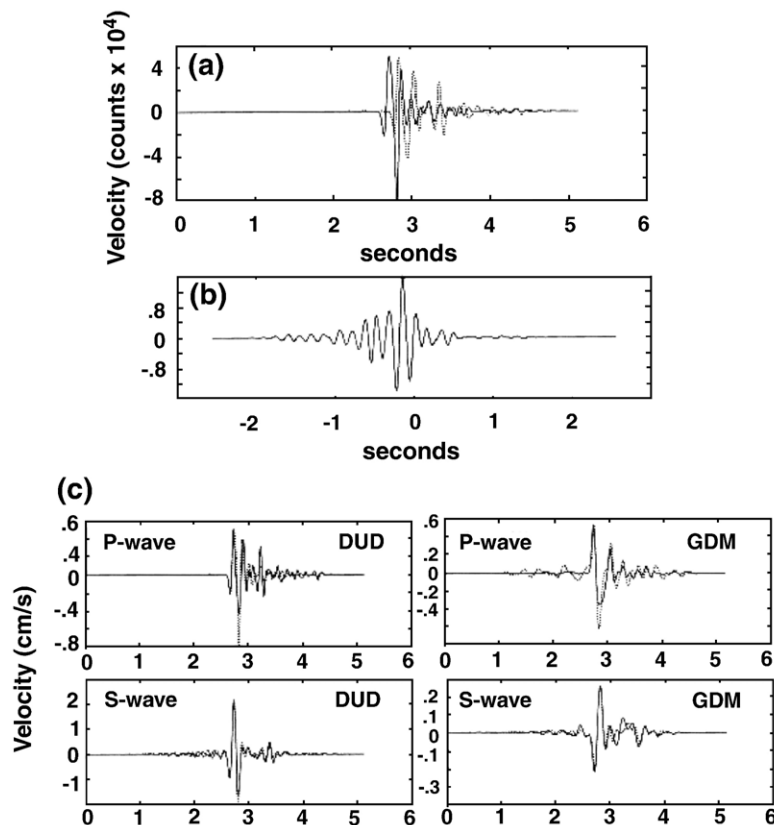


Fig. 4. a) P-wave window for two events plotted relative to the adjusted arrival time, b) normalized cross-correlation showing optimum lag time (differential travel time), and c) examples of P and S waves at two stations after adjustment by lag time.

The mean horizontal and vertical single 68% confidence estimates are 1.2 and 2.1 km, respectively, for the aftershocks (Fig. 2).

We have located 1238 aftershocks. Fig. 3a shows that the aftershocks are distributed over a fairly broad area, but that most epicenters fall within roughly trapezoidal shape with the parallel sides oriented east west. The northern edge at  $\sim 23.6^\circ$  is approximately 55 km long,

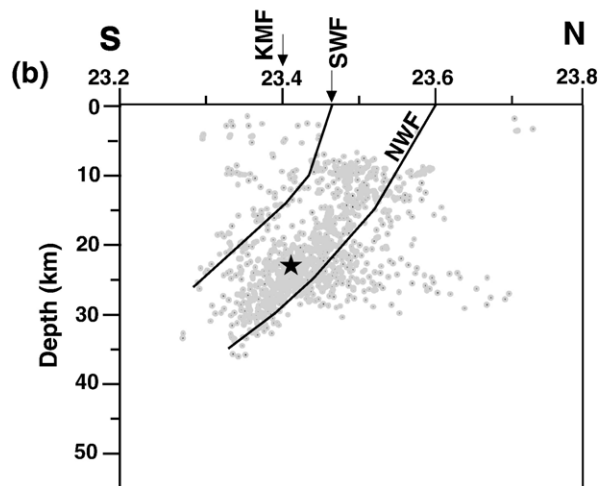
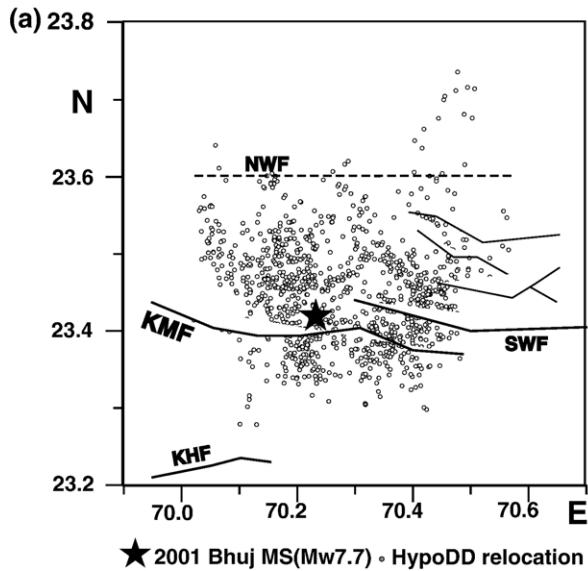


Fig. 5. (a) Relocated epicenters of selected 1172 aftershocks by using HYPODD, which have occurred during 12–28 February 2001. A solid star shows the epicenter for the 2001 Bhuj mainshock. The inferred causative fault is shown by dotted line and marked as NWF. (b) Hypocentral depth plots of selected earthquakes in N–S direction (Geologically valid inferred fault trace is shown by dotted line and marked as NWF. Arrows mark surface traces of KMF and SWF (after Biswas (1987)).

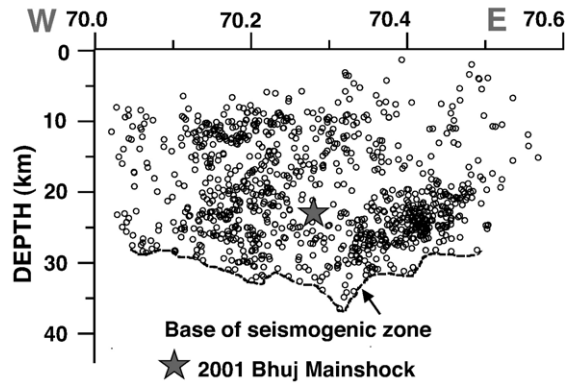


Fig. 6. Strike-parallel (E–W) depth profile of HYPODD relocated aftershocks illustrating short and long wavelength roughness at the base of the seismogenic zone. The dotted lines represent the approximate outline of the base of the seismogenic zone. And, the star mark denotes the hypocenter of the 2001 Bhuj mainshock.

and 5–10 km deep. The southern edge at  $\sim 23.3^\circ$  is approximately 25 km long and  $\sim 35$  km deep. In N–S cross-section (Fig. 3b) a distinct south-dipping concentration of aftershocks is seen to extend from between 3–10 km deep to about 35 km deep, which has been named as north Wagad fault (NWF) (Rastogi et al., 2001). The depth-distribution also shows the south dipping south Wagad fault (SWF), which is not obvious due to scatter in focal depth distribution. The east–west strike is about  $8^\circ$  from the WSW–ENE striking, south dipping, nodal plane of the mainshock (Fig. 1). The aftershocks are well south of the Island Belt fault, east of the Banni fault, and for the most part north of the surface trace of the Kachchh Mainland fault and (its apparent eastern extension) the Wagad fault. Earthquakes occurring outside the trapezoid are not on the mainshock fault plane.

### 5. Relocation of aftershocks using double-difference algorithm

To reduce the level of location uncertainty, we employed the double-difference earthquake location method, HYPODD (Waldhauser and Ellsworth, 2000). The method incorporates travel time differences formed from P- and S-wave arrival times with differential travel times derived from waveform cross-correlation methods. It is suggested that uncertainties are improved by an order of magnitude for two basic reasons (Waldhauser and Ellsworth, 2000). First, specifying the travel time as a double difference minimizes errors due to unmodeled velocity structure. In the Kachchh basin with slower Mesozoic sediments overlying a fast crystalline

basement, this could prove significant. Secondly, waveform cross-correlation measurements are potentially more accurate than picks made by an analyst, particularly for S waves where the onset is often obscured by the P-wave coda.

The HYPODD algorithm was developed to optimally relocate seismic events in the presence of measurements errors and earth model uncertainty (Waldhauser and Ellsworth, 2000). The fundamental equation of this iterative least-squares procedure relates the residual between the observed and predicted phase travel time difference for pairs of earthquakes observed at common stations to change in the vector connecting their hypocenters through the partial derivatives of the travel times

for each event with respect to the unknown. When the earthquake location problem is linearized using the double-difference equations, the common mode errors cancel, principally those related to the receiver-side structure. Thus, this algorithm does not require accounting for the station corrections or high-accuracy of predicted travel times for the portion of the ray path that lies outside the focal volume. This approach is especially useful in regions with a dense distribution of seismicity, i.e. where distances between neighboring events are only a few kilometers or less. The aftershock zone of 2001 Bhuj earthquake covers an area of 40 km × 70 km with 1238 earthquakes in a tight cluster. Therefore, HYPODD should work well to relocate Bhuj aftershocks.

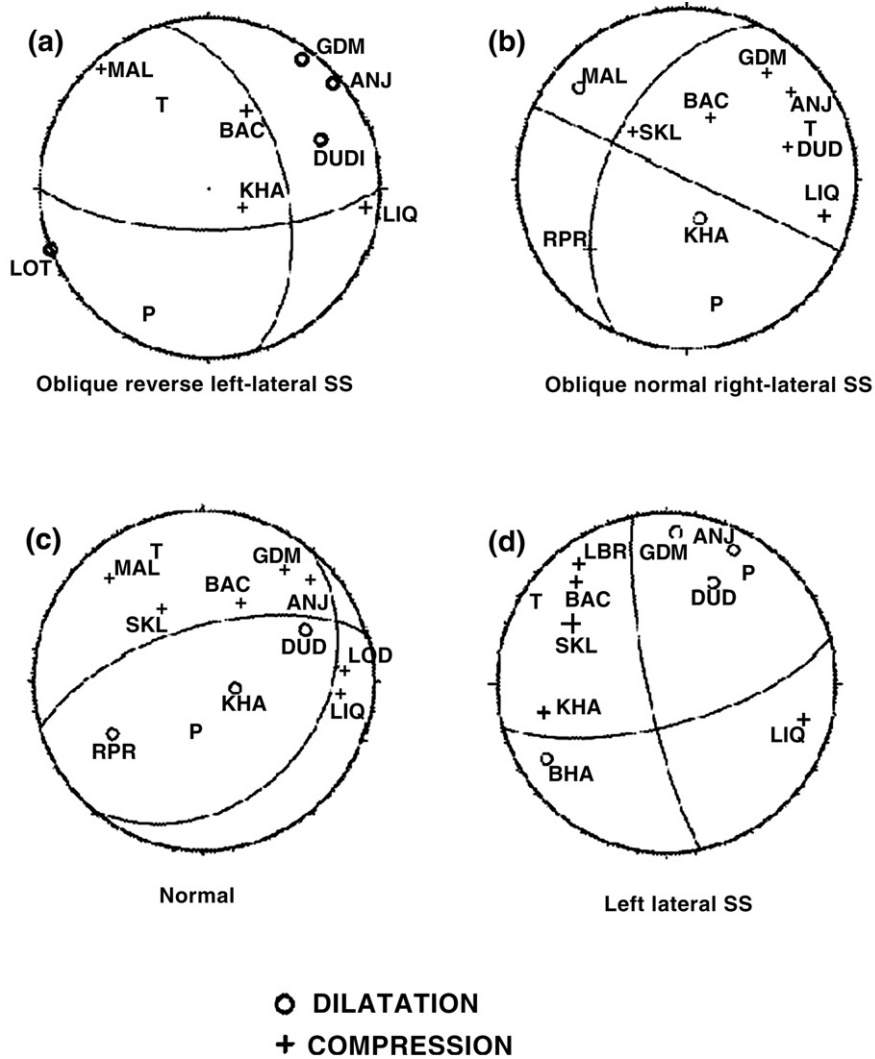


Fig. 7. Examples of different focal mechanism solutions obtained from more than 8 stations first P-motion data using FPFIT program (a) oblique reverse left lateral strike-slip, (b) oblique normal right lateral strike-slip, (c) normal, and (d) left lateral strike-slip.

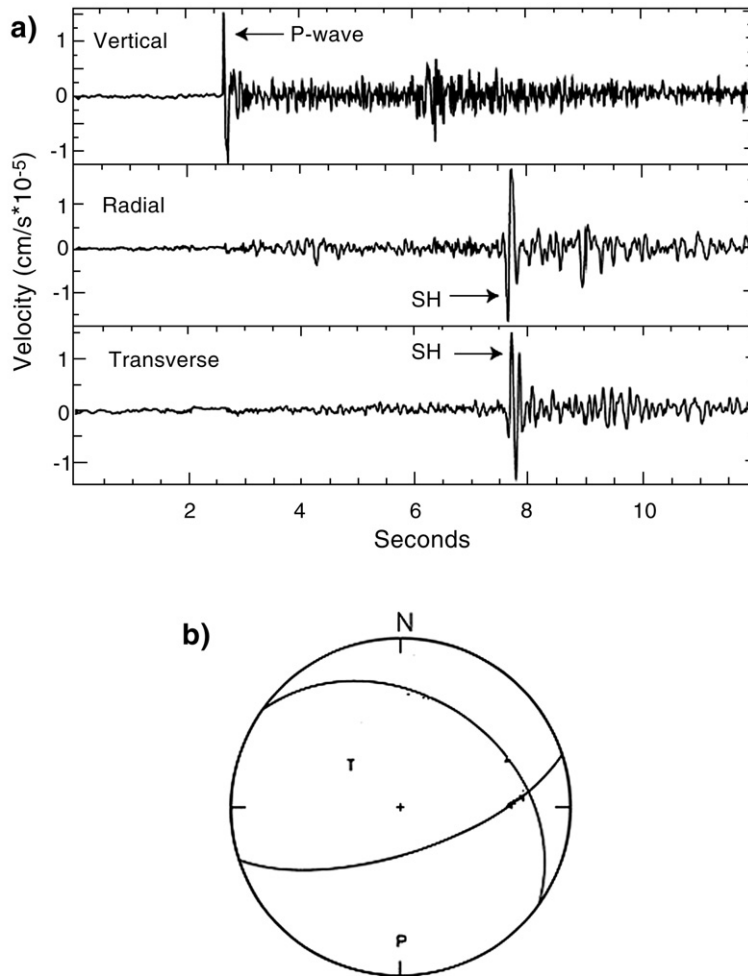


Fig. 8. a) Displacement waveforms at station GDM for event#37. Horizontal waveforms are rotated to radial and transverse allowing identification of S-wave polarity. (b) Focal mechanism for event#37. For the polarities, circles represent compressions and triangles represent dilatations.

Although, Waldhauser and Ellsworth (2000) used the cross-spectral method of Poupinet et al. (1984) to measure the differential travel times, we find this method to be unstable for radically dissimilar events. In this study a cross-correlation technique has been used that was found to be quite stable for analysis of broadband of waveforms (Horton et al., 2004). This method has been graphically illustrated in Fig. 4 where the P-waves from two events at site DUD are correlated. The data are bandpass-filtered between 0.1 and 6 Hz and a 5.12 second window is used. The windows are centered on the same specified time relative to the origin time of each event (Fig. 4a). The specified time corresponds to the travel time of the phase in question for the first event. The cross-correlation of the two time series is shown Fig. 4b. The differential travel-time corresponds to the lag time of the peak in the cross-correlation function. Only those measurements having a correlation coefficient

equal to or larger than 0.75, are used in the double difference earthquake location. The correlation coefficients are used to weight the uncertainty of the observations. The method has a precision of one sample, and it is a stable estimator since non-similar signals do not satisfy the correlation coefficient threshold. An example of correlated P and S waves at two stations from the same event are shown in Fig. 4c.

Travel time differences formed from both manually picked P- and S-wave arrival times and differential travel times derived from waveform cross-correlation methods as shown above can be used by HYPODD. We used a total of eight iterations for the conjugate gradient method (LSQR) within HYPODD inversion technique. In this study, the travel time differences have been estimated for all the event pairs with an inter-event separation less than 5 km and stations located in 100 km radius from the cluster centroid. A maximum of 6 to

8 neighboring events linked to each other were only considered for the relocation. The condition numbers (i.e. ratio of the largest to smallest eigen value) obtained for 8 iterations range from 41 to 70. HYPODD could relocate 1172 out of 1238 aftershocks, which were sufficiently clustered. The apriori weights assigned for P and S waves were 1.0 and 0.5, respectively. After four iterations weights were assigned for small inter event distances and vice versa to both the P and S phase data. We then checked each location obtained by LSQR against the singular value decomposition (SVD) result to insure consistency in hypocentral location (Waldhauser and Ellsworth, 2000). The average relative uncertainties for the aftershocks upon relocation are 30 m in epicentral location and 50 m in focal depth estimation.

The relocated epicenters using HYPODD are plotted in Fig. 5a that suggests significant differences in epicentral locations in comparison with the earlier location by HYPOELLIPSE (Fig. 3a). The mean of relative epicentral location uncertainty obtained by HYPODD is 30 m, which is quite less in comparison to the absolute epicentral location uncertainty of 1000 m as obtained by HYPOELLIPSE. The distribution of epicenters still defines an E–W trending aftershock zone covering almost  $40\text{ km} \times 60\text{ km}$  area, which is about  $8^\circ$  from the WSW–ENE striking nodal plane of the mainshock (Fig. 1). The relocated hypocenters delineate a distinct south dipping E–W trending aftershock zone extending up to 35 km depth, which involves a crustal volume of  $40\text{ km} \times 60\text{ km} \times 35\text{ km}$ . The N–S hypocentral depth

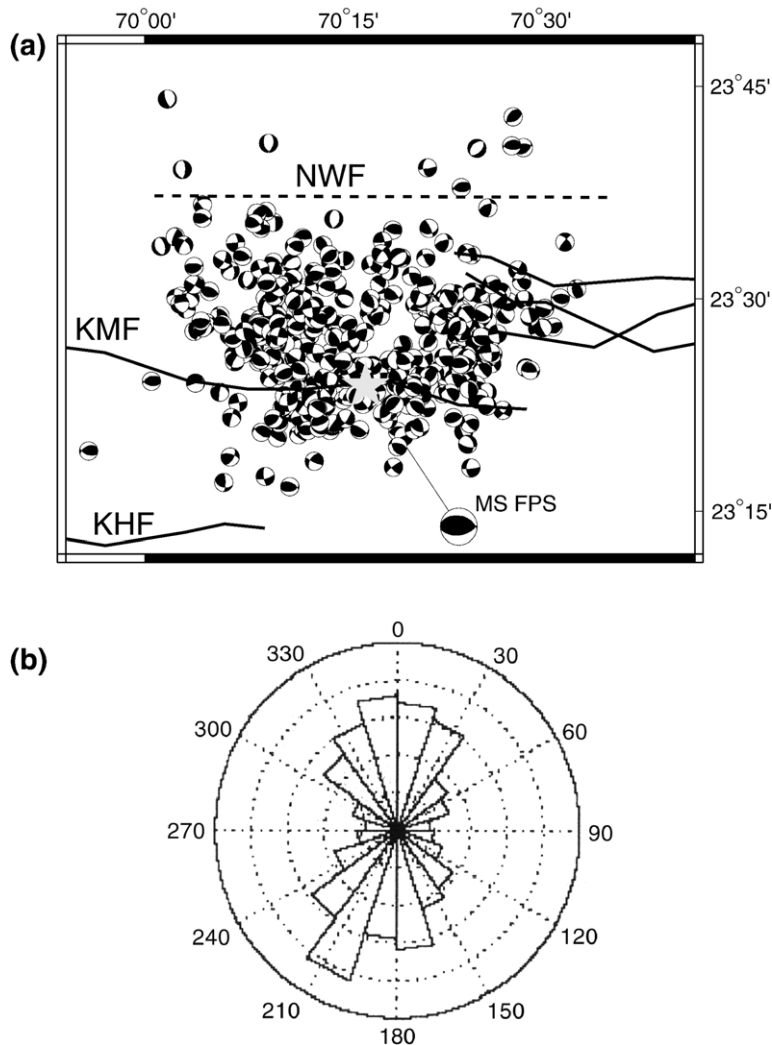


Fig. 9. (a) Spatial distribution of aftershock focal mechanisms inferred from first motion of P-waves using FPFIT as well as FOCMEC. MS FPS represents the fault plane solution of the 2001 Bhuj manishock. KTF represents the Katrol Hill Fault, and (b) Rose diagram for the earthquake focal mechanism P axes for selected 444 aftershocks.

distribution also clearly delineates the south-dipping south Wagad fault (SWF) at 3–25 km depth. A substantial compressing of the vertical distribution of hypocenters in comparison to earlier HYPOELLIPSE hypocentral location (Fig. 3b) is apparent in the transverse cross-section as shown in Fig. 5b. The mean of relative focal depth uncertainty obtained by HYPODD is 50 m, which is quite less in comparison to the absolute focal depth uncertainty of 2000 m as obtained by HYPOELLIPSE (Fig. 3b).

Strike-parallel (E–W) hypocentral depth section reveals that the base of seismogenic zone is irregular, with a variation in aftershock activity cutout depth of up to 7 km occurring on wavelength of ~10 to 60 km (Fig. 6). This observation suggests a significant variation in brittle/ductile transition depth beneath the aftershock zone where the earthquake foci in the both western and eastern ends are confined up to 28 km depth whilst in the central aftershock zone they are limited up to 35 km depth.

### 6. Aftershock focal mechanisms

We determined 991 focal mechanism solutions for Bhuj aftershocks using the program, FPFIT (Reasenber and Oppenheimer, 1985). FPFIT is a grid search routine that minimizes the misfit between nodal planes and observed first-motion data. From these, we selected 444 events having a single solution, a misfit less than 0.2, and less than 30° uncertainty in dip, rake and azimuth. Between 8 and 12 first motions were observed for these events. Few examples of different focal mechanism solutions determined by FPFIT are shown in Fig. 7(a–d).

For events where FPFIT produced multiple solutions, we used the program FOCMEC (Snoke et al., 1984). FOCMEC is also a grid search routine, however, it

Table 3  
Different faulting types

Rake angle	Type of faulting	Number
-157.5 > rake > 157.5	Right lateral strike-slip	46 (10%)
-112.5 > rake > -157.5	Oblique-normal right lateral strike-slip	32 (7%)
-67.5 > rake > -112.5	Normal	28 (6%)
-22.5 > rake > -67.5	Oblique-normal left-lateral strike-slip	33 (7.5%)
22.5 > rake > -22.5	Left-lateral strike-slip	56 (12.5%)
67.5 > rake > 22.5	Oblique-reverse left-lateral strike-slip	78 (18%)
112.5 > rake > 67.5	Reverse	106 (24%)
157.5 > rake > 112.5	Oblique-reverse right lateral strike-slip	65 (15%)

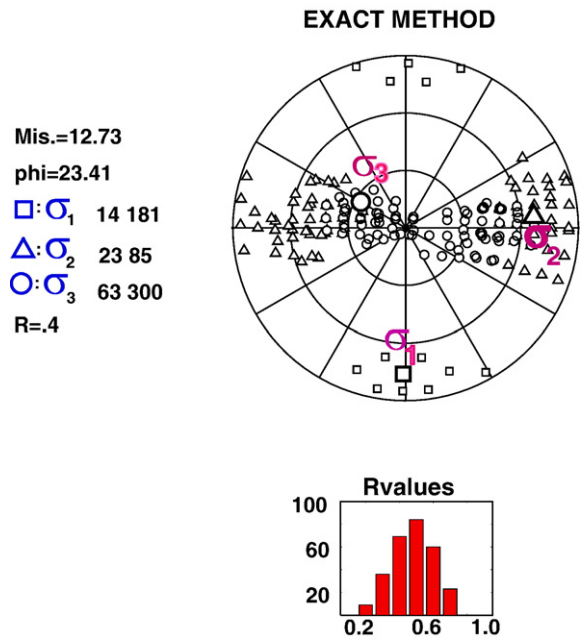


Fig. 10. Maximum principal stress axis,  $\sigma_1$  (square), intermediate axis,  $\sigma_2$  (triangle), and least principal axis,  $\sigma_3$  determined from inverting the P and T axes of focal mechanisms of selected 444 aftershocks by Exact method.

minimizes the misfit between possible nodal planes and broader observed data set. In addition to P-wave first motions, FOCMEC utilizes Sh, and Sv first-motion observations, and amplitude ratios Sv/Sh, Sh/P and Sv/P to constrain the possible focal mechanisms. An additional 41 events were added. To obtain these additional observations, the seismograms are rotated to radial and transverse components. Then, the P, Sh and Sv amplitudes were estimated from the vertical, transverse and radial component, respectively (Fig. 8a). Fig. 8b shows an example focal mechanism for an aftershock determined using FOCMEC and the larger set of constraints.

The aftershock focal mechanisms are shown in Fig. 9a. The solutions were sorted into faulting types based on rake angle following the convention of Aki and Richards (1965) and listed in Table 3. Because these classifications are based on the rake angle, it was necessary to fix the fault plane between the two nodal planes based on the geological information. For each focal mechanism solution, the fault plane was chosen as that nodal plane which agrees with the orientation of faults in the vicinity mapped or compiled by Biswas (1987). In most cases, the faulting type was the same regardless of which nodal plane was assumed to be the fault plane. A total of 143 events are oblique reverse, 106 reverse, 102 strike slip, 65 oblique normal, and 28 normal (Table 3; Fig. 7(a–d)). All types of focal mechanism are



observed although reverse and strike–slip mechanisms are dominant.

Reverse movement mainly characterizes these mechanisms with minor strike–slip component along a preferred south dipping plane, however, some mechanisms show east or west dipping planes. Some pure reverse and strike–slip mechanisms have also been noticed (as shown in Fig. 9a). These solutions suggest a dominant reverse movement with a strike slip component on a south dipping plane, which agrees with the causative nodal plane of the mainshock focal mechanism as shown in Fig. 9a (Antolik and Dreger, 2003).

Horizontal projections of the compression (*P*) axis show a wide scatter in orientation. However, a rose diagram, Fig. 9b, shows that the *P*-axes are centered on a nearly north–south orientation with about 40° of scatter to either side. Although a wide range of focal mechanism type are observed for aftershocks of the Bhuj earthquake, the dominant pattern is consistent with the prevailing north–south compression over the Indian

plate (Cloetingh and Wortel, 1986; Coblenz et al., 1998).

### 7. Stress inversion using focal mechanism estimates

The grid search inversion technique (Exact method), FMSI, of Gephart (1990a,b) has been used for the stress inversion using *P*- and *T*-axes of selected 444 focal mechanisms, which have P-wave first-motion data from 8–12 stations, misfit less than 0.2 and less than 30° uncertainty in dip, rake and azimuth (Fig. 9a). In this method, the misfit measures the minimum rotation about any axis, which will bring the fault plane into a position in which slip in the predicted direction would occur. The basic assumptions underlying the method are that the stress field is uniform in the region considered, that the focal mechanisms are independent of each other, and that slip takes place in the same direction as the resolved shear stress on the fault plane. Here, we applied uncertainties estimated from FPFIT to the first-motion data

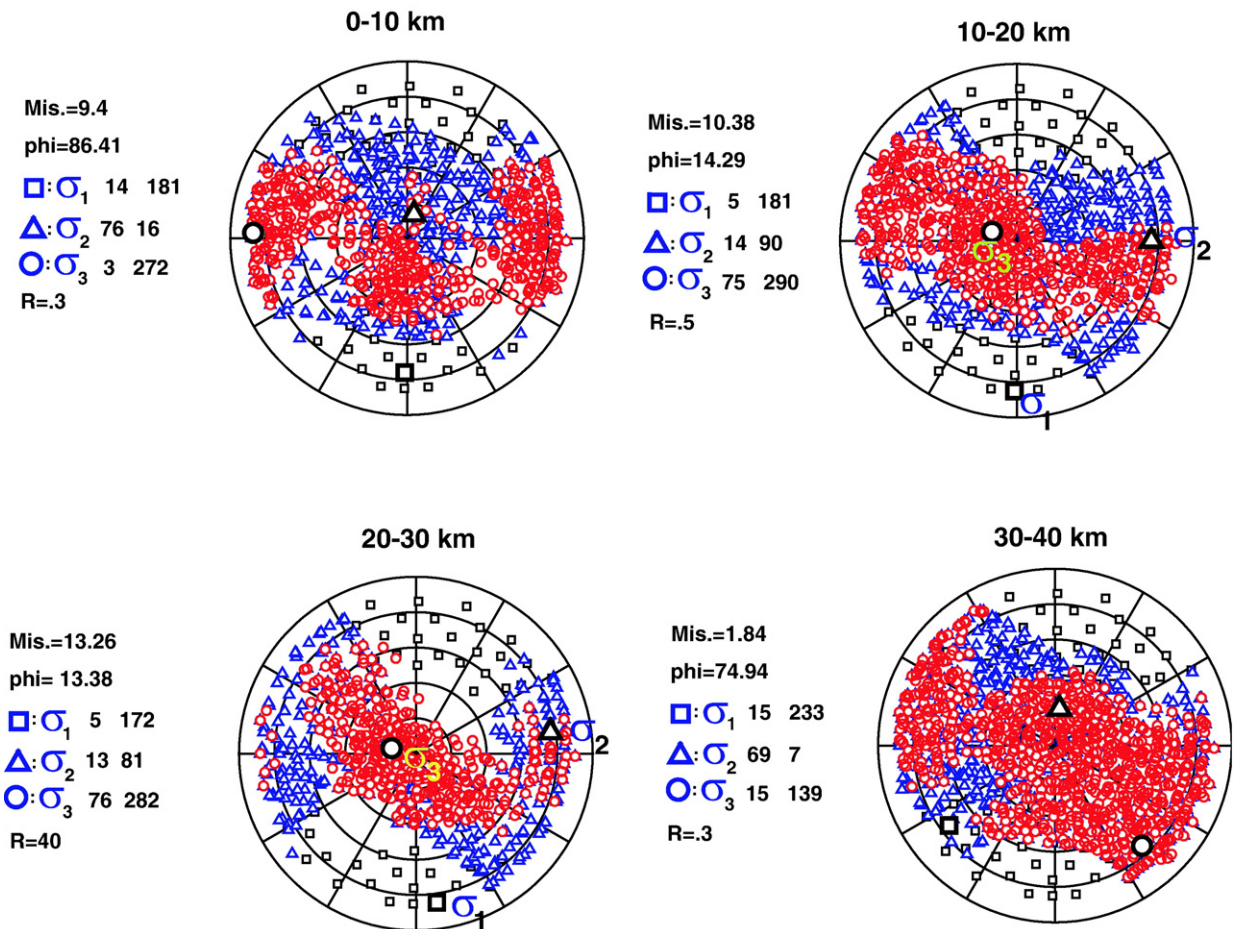


Fig. 12. Solutions of exact method stress inversion for four different depth bins (a) 0–10 km, (b) 10–20 km, (c) 20–30 km, and (d) 30–40 km.

to provide a better estimate of the true error in the stress tensor model. For the aftershock zone, the misfit and ratio,  $R [=(\sigma_2 - \sigma_1)/(\sigma_3 - \sigma_1)]$  obtained by the exact method are  $12.73^\circ$  and 0.4, respectively (Fig. 10). The large misfit of the order of  $12.73^\circ$  suggests a relatively more heterogeneous stress regime in the aftershock zone (Gillard et al., 1992). However, the stress inversion suggests an  $N181^\circ E$  oriented maximum principal stress with shallow dip of  $14^\circ$  corroborating well with the prevailing N–S orientation of the regional compression resulted from the northward movement of the Indian plate.

Spatial distribution of  $P$ -axes of selected 444 FPS shows a significant variation in  $P$ -axes orientation suggesting a heterogeneous distribution of numerous faults in the aftershock zone (Fig. 11a). The depth-wise distribution of  $P$ -axes with a bin of 10 km also suggests a significant variation in  $P$ -axes orientation at 0–30 km depth range, however, it suggests a dominant NE orientation at 30–40 km depth range (Fig. 11(b–e)). However, the stress inversion for the  $P$  and  $T$  axes from FPSs of four different depth bins (0–10, 10–20, 20–30 and 30–42 km) shows a N–S orientation for 0–10 ( $N181^\circ E$ ), 10–20 ( $N181^\circ E$ ) and 20–30 ( $N172^\circ E$ ) km depth bins, however, stress tensor orientation show a change in orientation at 30–40 km ( $N233^\circ E$ ) depth range (Fig. 12(a–d)). It would be important to mention here that we could use only available 5 events for the 30–40 km depth range.

## 8. Discussions and conclusions

The 2001 Bhuj earthquake located in the Mesozoic Kachchh basin which has been experiencing large intraplate earthquakes (Rajendran and Rajendran, 2001; Gupta et al., 2001). Existing seismological data suggests that the majority of Kachchh intraplate earthquakes can be attributed to the sudden movement along the E–W trending pre-existing reverse/thrust faults in response to the prevailing N–S compression due to the northward movement of the Indian plate (Chung and Gao, 1995; Biswas, 1987). Nevertheless, the region is characterized by several uplifts associated with gravity and magnetic highs, which are generally being attributed to the crustal intrusive bodies (Chandrasekhar and Mishra, 2002). The results from local earthquake tomography and inversion of teleseismic body waves suggest an ultramafic/a mafic high velocity crustal body beneath the aftershock zone (Mandal et al., 2004a; Antolik and Dreger, 2003). Hence, it is apparent from the above-discussion that the seismicity at Kachchh rift basin is due to a combination of regional tectonics and

local spatial variation of stresses associated with the tectonic structures, which were probably originated due to earlier rifting ( $\sim 160$  Ma), followed by Deccan volcanism (65 Ma) (Courillot et al., 1986; Coblenz et al., 1998).

In accordance with the above-mentioned seismological observations, precise and accurate relocated aftershocks (by HYPODD) delineate an E–W trending south dipping aftershock zone extending up to a depth of 35 km. The spatial distribution of relocated aftershocks suggests a tight E–W trending cluster involving an area of  $60 \text{ km} \times 40 \text{ km}$ . In comparison to earlier locations by HYPOELLISE technique, the uncertainty in epicentral location and focal depth estimation has been reduced significantly. The spatial distribution of HYPODD relocations clearly reveals that the deeper aftershocks are falling in the south of aftershock zone, whereas, the shallower aftershocks are lying in the north of aftershock zone (Fig. 5a). The sudden termination of aftershocks along a NW trend at the western edge of the rupture suggests that the rupture might have ran up against a near vertical structure beneath the western end of the aftershock zone (Bodin and Horton, 2004) where a NE trending coseismic/reactivated lineament has been mapped (Ghevariya and Sahu, 2001). At the eastern end, aftershocks show a similar behavior along a NNE trend, where WAGAD uplift/Great Rann boundary might be acting as a geometric barrier. At the eastern end, a N–S trending coseismic/reactivated lineament has also been mapped (Ghevariya and Sahu, 2001). Aftershocks also suggest a sudden termination along an E–W trend at the southern end, which perhaps indicates stoppage of rupture due to some vertical structure where an E–W trending coseismic/reactivated lineament has been mapped (Ghevariya and Sahu, 2001). It seems the sudden terminations of the powerful rupture in all directions suggest that the epicentral zone is bounded by the coseismic/reactivated lineaments (Ghevariya and Sahu, 2001). There is another possibility that there are vertical mafic intrusive bodies beneath the epicentral zone, which might be the reason for sudden terminations of aftershock activity (Chandrasekhar and Mishra, 2002; Mandal et al., 2004a).

Our accurately estimated focal depths reveals a variation in the depth of the deepest seismicity amongst the various fault segments, which is largely constrained by the seismicity patterns. The N–S hypocentral depth distribution reveals a distinct south-dipping plane extending up to 35 km depth, which agrees well with the nodal plane of the mainshock focal mechanism (Antolik and Dreger, 2003). They also clearly delineate the south-dipping SWF at 4–25 km depth. Strike-parallel (E–W)

hypocentral depth section reveals that the base of seismogenic zone is irregular, with a variation in aftershock activity cutout depth of up to 7 km occurring on wavelength of  $\sim 10$  to 60 km (Fig. 6). The maximum depth of seismogenic faulting can be interpreted as the transition from brittle faulting to plastic deformation (Sibson, 1984). The maximum depth at which crustal earthquakes occur depends on factors like geometry and mode of faulting, geothermal gradient, lithology, pore fluid pressure and strain rate (Sibson, 1984). There are few published heat flow measurements in Kachchh, Roy (2003) noted a somewhat higher than normal heat flow from the Bhuj earthquake source region (55–93 mW/m<sup>2</sup>), which suggests higher rather than lower deep crust temperatures unless heat production is unusually high in shallow rocks. Sibson (1984) has shown that a change in geothermal gradient along strike from 20° to 30 °C/km would cause the base of seismogenic zone to shallow by 4–6 km depending on rock type. Our results suggest a 7 km shallowing of the seismogenic base beneath the central aftershock zone where the 2001 mainshock took place.

In a review article (Maggi et al., 2000), demonstrated that the intraplate earthquakes in the continental areas around the world confines only to the crust up to Moho depth except for a single small (ML 3.8) isolated event at 90 km depth reported in the northern Utah (Zandt and Richards, 1979). However, the deepest earthquakes in the Indian shield crust beneath the rift zone like Narmada Son lineament (NSL) do occur to depths very close to the Moho (Singh et al., 1997). It would be important to mention here that the NSL region was shown to have two brittle–ductile transitions one at shallow ( $\sim 12$ –15 km) and another at deeper ( $\sim 20$ –25 km) depths in presence of crustal intrusive bodies (Manglik and Singh, 2002). They also suggested that crustal strength profile also varies laterally along the NSL. Recently, Li et al. (2002) computed the strength envelope for the western Indian plate assuming a 40 km thick granitic crust and a geotherm characterized by a steady-state surface heat flow of 60 mW/m<sup>-2</sup> (Pollack et al., 1993), which also revealed two brittle–ductile transitions one at 15 km and another at 40 km depths. Their study also revealed that the crustal rheology is playing a very important role in controlling the lateral change in the crustal strength and the strong upper-middle crust can support most deviatoric stresses. It is well known that the crustal strength mainly depends on the crustal thermal state, but it also depends on the rheological effects of water contained in the hydrous minerals, where even small concentrations of a few tens of parts per million can greatly decrease the strength (Brace and Byerlee, 1970; Sibson, 1982;

Mackwell et al., 1998). In many regions, the continental Mantle has been metasomatized by small amount of a melt that is very enriched in hydrogen (Harte et al., 1993). Alternatively, from the above-discussion it could be inferred that the variation in seismogenic depths beneath the old Kachchh rift zone can also be explained in terms of changes in the rheological composition of the crustal materials.

The tomographic study revealed high velocity mafic intrusives on the eastern and western sides of the central aftershock zone (Mandal and Pujol, 2006). The modeling of gravity and magnetic data indicates a crustal thickening of 8–10 km resulted from the existence of volcanic plugs of alkaline magmatic composition beneath the epicentral zone of the 2001 Bhuj earthquake (Chandrasekhar and Mishra, 2002). Therefore, the compositional changes due to the intruded mafic intrusives can lead to a marked variation in the thermal state or rheological properties in the aftershock zone, which can explain the 7 km deepening of the seismogenic base. Hence, the deepest portion of the base of the seismogenic zone beneath the central fault segment will be the maximum probable zone for the future frictional failure (where the 2001 Mw 7.7 Bhuj mainshock took place).

In Kachchh region, the tomographic studies also revealed the presence of fluid-filled fractured rock matrix at 23–25 km depth, which is characterized by high crack density, high saturation rate and high porosity, which could enhance the fluid pressure resulting in lubrication of the fault zone (Mishra and Zhao, 2003; Mandal et al., 2004b). Further, the upward advection of fluids along fractures could locally raising the temperature along the fault zone (Bickle and McKenzie, 1987; Hoisch, 1991), which could also provide an alternative explanation for the 7 km change in the seismogenic base along the north Wagad fault zone.

The Kachchh region is located in Mesozoic rift environment that was earlier characterized by tensional stresses, however, the focal mechanism solutions of earthquakes during last few decades show a dominant compressive regime with almost N–S trending *P*-axes (Chung and Gao, 1995; Antolik and Dreger, 2003). Thus, present day compressive stress regime suggests that this region is undergoing a stage of inversion tectonics (Antolik and Dreger, 2003). The deformation data suggests that the Indian subcontinent is moving northward at a rate of approximately 52 to 63 mm/yr, and is colliding with the northward moving Asian plate (Burgmann et al., 2001). The forces related to this collision apparently control the current pattern of tectonic activity in India, which led to domination of

northward compression over the Indian plate. Recent modeling of intraplate stresses and GPS studies for Indian region showed on an average a dominant N–S compression over the Indian plate due to the northward movement of the Indian plate (Cloetingh and Wortel, 1986; Coblenz et al., 1998; Bilham, 1999; Paul et al., 2001). In general, major east–west trending regional tectonic structures/faults characterize the Kachchh region, which were reactivated in the Mesozoic and Cenozoic time resulting in the formation of basin (Biswas, 1987). These E–W trending structures perhaps indicate an E–W extension for the region, which is consistent with extension direction determined from geodetic measurements (Bendick et al., 2001). The estimated focal mechanism solutions for 444 selected aftershocks suggest a dominant reverse movement with a strike slip component on a preferred south-dipping plane. Some pure dip slip solutions were also determined. Specifically, focal mechanism *P* axes trend N–S in the vicinity of the mainshock epicenter and rotate to NNE–SSW or NNW–SSE away from it.

In accordance with the prevailing N–S compressive stress regime, the exact method of stress inversion of 444 selected focal mechanism solutions reveals that the axis of maximum principal stress is oriented N181°E with a shallow dip (=14°). The orientation agrees with the *P*-axes orientation obtained from the focal mechanism solution of mainshock (strike N181° E, plunge 5°) as suggested by waveform inversion of teleseismic body waves (Antolik and Dreger, 2003; Figs. 1 and 10). The stress ellipsoid is oblate ( $R=0.4$ ). The pattern of stresses obtained from stress inversion suggests that the prevailing compressive stress regime in the region will prefer thrust/reverse mechanism (because  $\sigma_1$  and  $\sigma_2$  are almost horizontal and  $\sigma_3$  is almost vertical (Fig. 10)). This result is in good agreement with the available seismological, geophysical and geological information of the area (N–S orientation of *P*-axes for focal mechanism solution of 1956 Anjar earthquake (Chung and Gao, 1995), E–W trending major faults suggesting E–W extension thus N–S compression (Biswas and Khattri, 2002), N–S compression from GPS and modeling of regional plate stresses (Cloetingh and Wortel, 1986; Coblenz et al., 1998; Bendick et al., 2001)). This indicates that the stress field in Kachchh, Gujarat, India is relatively uniform and that the maximum principal stress has an orientation N–S that might be predicted on the basis of current plate motions or from the directions of the *P*-axes of the earthquakes (Cloetingh and Wortel, 1986; Chung and Gao, 1995; Coblenz et al., 1998; Bendick et al., 2001; Burgmann et al., 2001).

The spatial distribution and stress inversions of different depth bins of the *P* and *T* axes of selected aftershocks suggest a heterogeneous stress regime (as indicated by large misfit values >9°) with a dominant consistent N–S orientation of the *P*-axes at 0–30 km depth range, except a homogeneous stress regime with a rotation (N233° E) in *P*-axes orientation at deeper (30–40 km) crustal depths. Further, the estimated large misfit values (>6°) at 0–30 km depth range, also indicates a heterogeneous stress regime resulted from the existence of varied nature and orientation of fractures and faults as revealed by the accurately relocated hypocenters of aftershocks. However, the change in stress tensor orientation and homogeneous stress regime as indicated by a minimum misfit of 1.89° at deeper depths (30–40 km) could be explained in terms of the domination of the prevailing N30° E orientation of the homogeneous regional northward compression due to the northward motion of Indian plate.

### Acknowledgements

The authors are thankful to Dr. V. P. Dimri, Director, NGRI for his encouragement and kind permission to publish this work. The first author is grateful to Central Scientific and Industrial Research, India for providing the Raman Research Fellowship to carry out this work. Authors are grateful to CERI, Memphis, USA and Hirosaki University of Japan for providing their aftershock phase data.

### References

- Aki, K., Richards, P.G., 1965. *Quantitative Seismology*. W.H. Freeman, New York.
- Antolik, M., Dreger, D.S., 2003. Rupture process of the 26 January 2001 Mw 7.6 Bhuj, India, earthquake from teleseismic broadband data. *Bull. Seismol. Soc. Am.* 93, 1235–1248.
- Bendick, R., Bilham, R., Fielding, E., Gaur, V.K., Hough, S.E., Kier, G., Kulkarni, M.N., Martin, S., Mueller, K., Mukul, M., 2001. The 26 January 2001 “Republic Day” earthquake, India. *Seismol. Res. Lett.* 72, 328–335.
- Bickle, M.J., McKenzie, D., 1987. The transport of heat and matter by fluids during metamorphism. *Contrib. Mineral. Petrol.* 95, 384–392.
- Bodin, P., Horton, S., 2004. Source parameters and tectonic implications of aftershocks of the Mw7.6 Bhuj earthquake of January 26, 2001. *Bull. Seismol. Soc. Am.* 94, 818–827.
- Bodin, P., Horton, S., Johnston, A.C., Withers, M., Langston, C., Chiu, J.M., Budhbhatti, K., Gombert, J., 2001. Aftershocks of the Gujarat, India Republic Day earthquake. *Seismol. Res. Lett.* 72, 372–397.
- Bott, M.H.P., 1959. The mechanics of oblique slip faulting. *Geol. Mag.* 96, 109–117.
- Brace, W.F., Byerlee, J.D., 1970. California earthquakes Why only shallow focus? *Science* 168, 1573–1576.

- Bureau of Indian Standards, 2002. Criteria for Earthquake Resistant Design of Structures (Fifth Revision). 39 pp.
- Biswas, S.K., 1987. Regional framework, structure and evolution of the western marginal basins of India. *Tectonophysics* 135, 302–327.
- Biswas, S.K., Khattri, K.N., 2002. A Geological study of earthquakes in Kutch, Gujarat, India. *J. Geol. Soc. India* 60, 131–142.
- Bilham, R., 1999. Slip parameters for the Rann of Kachchh, India, 16 June 1819 earthquake quantified from contemporary accounts. In: Stewart, I.S., Vita-Finzi, C. (Eds.), *Coastal Tectonics*. Geological Society of London, vol. 146, pp. 295–318.
- Burgmann, P.J., Gaur, V.K., Bilham, R., Larson, K.N., Ananda, M.B., Jade, S., Mukul, M., Anupama, T.S., Satyal, G., Kumar, D., 2001. The motion and active deformation of India. *Geophys. Res. Lett.* 28 (4), 28–32.
- Chandrasekhar, D.V., Mishra, D.C., 2002. Some geodynamic aspects of Kutch basin and seismicity: an insight from gravity studies. *Curr. Sci.* 83, 492–498.
- Chung, W.Y., Gao, H., 1995. Source Parameters of the Anjar earthquake of July 21, 1956, India and its seismotectonic implications for the Kutch rift basin. *Tectonophysics* 242, 281–292.
- Cloetingh, S.A.P.L., Wortel, M.J.R., 1986. Stresses in the Indo-Australian plate. *Tectonophysics* 132, 49–67.
- Coblentz, D.D., Zhou, S., Hillis, R.H., Richardson, R.M., Sandiford, M., 1998. Topography, boundary forces, and the Indo-Australian intraplate stress field. *J. Geophys. Res.* 103, 919–931.
- Courtillot, V., Besse, J., Vandamme, D., Montigny, R., Jaeger, J.J., Cappetta, H., 1986. Deccan flood basalts at the Cretaceous–Tertiary boundary? *Earth Planet. Sci. Lett.* 80, 361–374.
- Dodge, D., 1996. Microearthquake studies using cross-correlation derived hypocenters, Ph.D. thesis, Stanford University, 146 pp.
- Foxall, W., Michelini, A., McEvilly, T.V., 1993. Earthquake travel time tomography of the southern Santa Cruz Mountains: control of fault rupture by lithological heterogeneity of the San Andreas fault zone. *J. Geophys. Res.* 98, 17,691–17,710.
- Gephart, J.W., 1990a. Stress and the direction of slip on fault planes. *Tectonics* 9, 845–858.
- Gephart, J.W., 1990b. FMSI: A FORTRAN program for inverting fault/slickenside and earthquake focal mechanism data to obtain the regional stress tensor. *Comput. Geosci.* 16, 953–989.
- Gephart, J.W., Forsyth, D.W., 1984. An improved method for determining the regional stress tensor using earthquake focal mechanism data: application to the San Fernando earthquake sequence. *J. Geophys. Res.* 89, 9305–9320.
- Ghevariya, Z.G., Sahu, B.K., 2001. Assessment of active faults and lineaments in Kutch and Saurashtra regions of Gujarat — A post 26 January 2001 Earthquake study. *Geol. Soc. Ind. Spec. Publ.* 65 (ii), 103–113.
- Gillard, D., Wyss, M., Nakata, J.S., 1992. A Seismotectonic model for Western Hawaii based on stress tensor inversion from fault plane solutions. *J. Geophys. Res.* 97, 6629–6641.
- Got, J.L., Frechet, J., Klein, F.W., 1994. Deep fault plane geometry inferred from multiple relative relocation beneath the south flank of Kilauea. *J. Geophys. Res.* 99, 15375–15386.
- Gowd, T.N., Srirama Rao, S.V., Gaur, V.K., 1992. Tectonic stress field in the Indian subcontinent. *J. Geophys. Res.* 97, 11,879–11,888.
- Gupta, H.K., Harinarayana, T., Kousalya, M., Mishra, D.C., Mohan, I., Purnachandra Rao, N., Raju, P.S., Rastogi, B.K., Reddy, P.R., Sarkar, Dipankar, 2001. Bhuj earthquake of 26 January 2001. *J. Geol. Soc. India* 57, 275–278.
- Harte, B., Hunter, R.H., Kinny, P.D., 1993. Melt geometry, movement and crystallization in relation to mantle dikes, veins and metamorphism. *Philos. Trans. R. Soc. Lond., A Contain. Pap. Math. Phys. Character* 342, 1–21.
- Hoisch, T.D., 1991. The thermal effects of pervasive and channelized fluid flow in the deep crust. *J. Geol.* 99, 69–80.
- Horton, S.P., Kim, W.Y., Withers, M., 2004. The 6 June 2003 Bardwell, Kentucky, Earthquake Sequence: evidence for a locally perturbed stress field in the Mississippi Embayment. *Bull. Seismol. Soc. Am.* 95 (2), 431–445.
- Jaeger, J.J., Courtillot, V., Tapponnier, P., 1989. Paleontological view of the ages of the Deccan Traps, the Cretaceous/Tertiary boundary, and the India–Asia collision. *Geology* 17, 316–319.
- Johnston, A.C., 1994. Seismotectonic interpretations and conclusions from the stable continental regions. *The Earthquakes of Stable Continental Regions: Assessment of Large Earthquake Potential*. Electric Power & Research Institute, Palo Alto. Report TR 10261 ch.3.
- Kissling, E., 1995. *Velost Users Guide*, Internal report, Institute of Geophysics, ETH Zurich, pp. 26.
- Lahr, J.C., 1995. HYPOELLIPSE Y2K: A computer program for determining local earthquake hypocentral parameters, magnitude, and first-motion pattern. *Open-File Rep. U. S. Geol. Surv.* 99-023, 112 pp.
- Li, Q., Liu, M., Yang, Y., 2002. The 01/26/2001 Bhuj, India, Earthquake: Intraplate or Interplate? In: Stein, S., Freymuller, G. (Eds.), *Plate Boundary Zones*, AGU Geophysical Monograph, pp. 255–264.
- Maggi, A., Jackson, J.A., McKenzie, D., Priestley, K., 2000. Earthquake focal depths, effective elastic thickness, and the strength of the continental lithosphere. *Geology* 28, 495–498.
- Mackwell, S.J., Zimmermann, M.F., Kohlsedth, D.I., 1998. High-temperature deformation of dry diabase with application to tectonics on Venus. *J. Geophys. Res.* 103, 975–984.
- Mandal, P., in press. Sediment Thicknesses and Qs vs. Qp relations in the Kachchh rift basin, Gujarat, India using Sp converted phases, *Pure Appl. Geophys.*
- Mandal, P., Pujol, J., 2006. Seismic imaging of the aftershock zone of the 2001 Mw7.7 Bhuj earthquake. *Geophys. Res. Lett.* 33 (L05309), 1–4.
- Mandal, P., Rastogi, B.K., Satyanarayana, H.V.S., Kousalya, M., Vijayaraghavan, R., Satyamurthy, C., Raju, I.P., Sarma, A.N.S., Kumar, N., 2004a. Characterization of the causative fault system for the 2001 Bhuj earthquake of Mw 7.7. *Tectonophysics* 378, 105–121.
- Mandal, P., Rastogi, B.K., Satyanarayana, H.V.S., Kousalya, M., 2004b. Results from Local Earthquake Velocity Tomography: Implications toward the Source Process Involved in Generating the 2001 Bhuj Earthquake in the Lower Crust beneath Kachchh (India). *Bull. Seismol. Soc. Am.* 94 (2), 633–649.
- Manglik, A., Singh, R.N., 2002. Thermomechanical structure of the central Indian shield: constraints from deep crustal seismicity. *Curr. Sci.* 82, 1151–1157.
- McGarr, A., Gay, N.C., 1978. State of stress in the Earth's crust. *Annu. Rev. Earth Planet. Sci.* 6, 405–436.
- McKenzie, D.P., 1969. The relation between fault plane solutions for earthquakes and the directions of the principal stresses. *Bull. Seismol. Soc. Am.* 59, 591–601.
- Michelini, A., 1991. Fault zone structure determined through the analysis of earthquake arrival times, Ph.D. thesis, Univ. of California, Berkeley.
- Michael, A.J., Eberhart-Phillips, D., 1991. Relations among fault behavior, subsurface geology, and three-dimensional velocity models. *Science* 253, 651–654.

- Mishra, O.P., Zhao, D., 2003. Crack density, saturation rate and porosity at the 2001 Bhuj, India, earthquake hypocenter: a fluid-driven earthquake? *Earth Planet. Sci. Lett.* 212, 393–405.
- Negishi, H., Mori, J., Sato, H., Singh, R.P., Kumar, S., 2001. Aftershocks and slip distribution of Mainshock, A comprehensive survey of the 26 January 2001 earthquake (Mw 7.7) in the state of Gujarat, India. *Research Report on Natural Disasters*, pp. 33–45. December.
- Paul, J., Burgmann, R., Gaur, V.K., Bilham, R., Larson, K.M., Ananda, M.B., Jade, S., Mukul, M., Anupama, T.S., Satyal, G., Kumar, D., 2001. The motion and active deformation of India. *Geophys. Res. Lett.* 28, 647–651.
- Patriat, P., Achache, J., 1984. India–Eurasia collision chronology has implications for crustal shortening and driving mechanism of plates. *Nature* 311, 615–621.
- Pollack, H.N., Hunter, S.J., Johnson, J.R., 1993. Heat flow from the Earth's interior: analysis of the global data set. *Rev. Geophys.* 31, 267–280.
- Poupinet, G., Ellsworth, W.L., Frechet, J., 1984. Monitoring velocity variations in the crust using earthquake doublets: an application to the Calaveras fault, California. *J. Geophys. Res.* 89, 5719–5731.
- Pujol, J., 1988. Comments on the joint determination of hypocenters and station corrections. *Bull. Seismol. Soc. Am.* 78, 1179–1189.
- Rajendran, C.P., Rajendran, K., 2001. Character of deformation and past seismicity associated with the 1819 Kachchh earthquake, northwestern India. *Bull. Seismol. Soc. Am.* 91 (3), 407–426.
- Rastogi, B.K., Gupta, H.K., Mandal, P., Satnarayana, H.V.S., Kousalya, M., Raghavan, R., Jain, R., Sarma, A.N.S., Kumar, N., Satyamurty, C., 2001. The deadliest stable continental region earthquake occurred near Bhuj on 26 January 2001. *J. Seismol.* 5, 609–615.
- Reasenber, P.A., Oppenheimer, D., 1985. FPFIT, FPLOT and FPPAGE: Fortran computer programs for calculating and displaying earthquake fault-plane solutions. *Open-File Rep. U. S. Geol. Surv.* 85–739.
- Reddy, P.R., Sarkar, D., Sain, K., Mooney, W.D., 2001. A report on a collaborative scientific study at USGS, Menlo Park, USA (30th September–1st December 2001) (19 pp.).
- Richards-Dinger, K.B., Shearer, P.M., 2000. Earthquake locations in southern California obtained using source — specific station terms. *J. Geophys. Res.* 105, 10939–10960.
- Roy, A.B., 2003. Geological and geophysical manifestations of the Reunion plume-Indian lithosphere interactions: evidence from northwest India. *Gondwana Res.* 6, 487–500.
- Schweig, E., Gomberg, J., Petersen, M., Ellis, M., Bodin, P., Mayrose, L., Rastogi, B.K., 2003. The M7.7 Bhuj earthquake: global lesson for earthquake hazard in intra-plate regions. *Geol. Soc. Ind.* 61, 277–282.
- Sibson, R.H., 1982. Fault zone models, heat flow, and the depth distribution of earthquakes in the continental crust of the United States. *Bull. Seismol. Soc. Am.* 72, 151–163.
- Sibson, R.H., 1984. Roughness at the base of the seismogenic zone: contributing factors. *J. Geophys. Res.* 89, 5791–5799.
- Singh, D., Alat, C.A., Singh, R.N., Gupta, V.P., 1997. Source rock characteristics and hydrocarbon generating potential of Mesozoic sediments in Lodhika Area, Saurashtra Basin, Gujarat, India. *Proceedings Second Int. Pet. Conference and Exploration Petrotech-97*, New Delhi, India, pp. 205–220.
- Snoke, J.A., Munsey, J.W., Teague, A.C., Bollinger, G.A., 1984. A program for focal mechanism determination by combined use of polarity of SV-P amplitude ratio data. *Earthq. Notes* 55 (3), 15–20.
- Sridevi, J., Mukul, M., Parvez, I.A., Ananda, M.B., Kumar, P.D., Gaur, V.K., 2001. Estimates of co-seismic displacement and post-seismic deformation using Global Positioning system geodesy for the Bhuj earthquake of 26 January, 2001. *Curr. Sci.* 82, 748–752.
- Thurber, C.H., 1983. Earthquake locations and three-dimensional crustal structure in the in the Coyote lake area, Central California. *J. Geophys. Res.* 88, 8226–8236.
- Waldhauser, F., Ellsworth, W.L., 2000. A double-difference earthquake location algorithm: method and application to the northern Hayward fault. *Bull. Seismol. Soc. Am.* 90, 1353–1368.
- Zandt, G., Richards, W.D., 1979. An upper mantle earthquake beneath the middle Rocky Mountains in NE Utah [abs.]. *Earthq. Notes* 50, 69–70.
- Zhao, D., Kanamori, H., Negishi, H., Wiens, D., 1996. Tomography of the Source area of the 1999 Kobe earthquake: evidence for fluids at the hypocenter? *Science* 274, 1891–1894.